

# Quadruped Pronking on Compliant Terrains Using a Reaction Wheel\*

Vasileios Vasilopoulos<sup>1</sup>, *Student Member, IEEE*, Konstantinos Machairas<sup>2</sup>, *Student Member, IEEE*,  
and Evangelos Papadopoulos<sup>2</sup>, *Senior Member, IEEE*

**Abstract**— While legged locomotion is a rapidly advancing area in robotics, several issues regarding the performance of such robots on deformable ground are still open. In this paper, we generate a pronking gait on a quadruped robot using a controller, which takes into account the effects of ground deformation. The controller, initially developed for monopods, is modified appropriately to operate for quadrupeds. The robot uses a reaction wheel to retain a desired body pitch. The dynamic models of leg motor drivetrains and of the reaction wheel are incorporated and their importance in the design of legged robots is highlighted. Simulation results show good performance in reaching commanded apex heights and forward velocities when traversing various deformable terrains, demonstrating that the developed controller is quite promising.

## I. INTRODUCTION

A most significant challenge in the field of legged robotics is the development of control algorithms that allow legged robots to traverse any type of terrain, while retaining desired motion characteristics. However, control requirements are demanding, especially when the terrain profile is rough. With these in mind, a common control strategy used by quadrupeds for traversing rough terrains involves footstep planning. LittleDog has presented significant results on uneven terrain [1]. However, it is capable of static walking only. StarLETH also uses a similar approach [2]; a foot placement algorithm along with distribution of virtual forces among the stance legs is used to reject perturbations from the environment.

Despite the increasing complexity of control algorithms for legged robots, many studies do not consider the effect of terrain compliance and permanent deformations. For example, researchers working on MIT's Cheetah 2 determine a target ground force profile according to the desired duty cycle and stride duration, [3]. The terrain is considered stiff and completely even. The effects of compliant terrains were taken into account in our recent work in which we developed a novel energy-based controller for a monopod hopping robot running over compliant terrains, using only one actuator [4].

It is usual to model the foot-terrain interaction of legged robots as a revolute joint. However, in this way, the effects of contact constraints and of terrain compliance on motion performance remain hidden. A number of steps are necessary

to assess such effects. For example, a viscoelastic model was used in [5], while a terradynamics approach was employed in [6]. A viscoplastic model has been proposed, which enables the assessment of the effects of terrain permanent deformations by taking into account various realistic parameters such as compaction in fast dynamic walking [4].

Another critical element in legged locomotion control schemes is the control of body attitude; tasks such as jumping over obstacles, rapid turning while running, and generally recovering from unexpected disturbances, require that the robot is capable of performing complex maneuvers in the aerial phase. So far, attitude control is mostly achieved indirectly through leg motion in the stance or in the aerial phase [7], [8], indicating that a tail-like system similar to that in animals is not always necessary. However, this technique assigns more control tasks to the legs, and thus it may not be optimal when the robot tries to fulfill more demanding tasks. Herein, as well as in numerous recent studies [9], [10], it is proposed that a dedicated tail-like appendage can be usefully incorporated in a legged robot to aid in reorientation maneuvers and enrich the repertoire of robot capabilities. Nevertheless, the additional capabilities must be traded off against the additional weight and power consumption.

In this paper we focus on a quadruped robot running on compliant terrain using a reaction wheel to control its body attitude. Using detailed actuator models, we highlight the importance of the limits imposed by the gearboxes and servoamplifiers, and examine their effect on quadruped motion by generating realistic gait simulations. The concept of virtual actuators is introduced that must be considered in models with virtual legs. To generate a pronking controller for maintaining a desired apex height and forward speed, the quadruped behavior is correlated to that of a monopod robot during stance. Simulation results show that the necessary periodic motion of both the body attitude and the reaction wheel during dynamic quadruped running is guaranteed, even in the presence of terrain compliance.

## II. QUADRUPED DYNAMIC MODEL

We introduce a planar model of a quadruped consisting of a body, two hip-actuated compliant legs and a reaction wheel. The legs represent the hind and fore leg pairs (virtual legs). It is assumed that when a foot impacts the ground, a point contact occurs and that bulldozing effects can be neglected.

*Model description.* The model shown in Fig. 1 consists of a main body with length  $2d$ , mass  $m_b$  and moment of inertia (MoI)  $I_b$  about its Center of Mass (CoM). Each leg CoM is in the middle of its length. Each virtual leg has mass  $m_l$ , MoI  $I_l$ , a prismatic compliant joint with stiffness  $k$  and is driven by a hip actuator, i.e. torques  $\tau_f$  and  $\tau_h$  for the fore and hind leg respectively. The reaction wheel is hinged at its CoM and has mass  $m_r$ , radius of gyration  $R$  and MoI  $I_r$ :

\* This research has been financed by the European Union (European Social Fund – ESF) and Greek funds through the Operational Program “Education and Lifelong Learning” of the National Strategic Reference Framework (NSRF) – Research Program: ARISTEIA: Reinforcement of the interdisciplinary and/or inter-institutional research and innovation.

The presentation of this paper was partially made possible through a travel grant by the “C. Mavroidis Award of Excellence in Robotics and Automation” at the NTUA.

<sup>1</sup>Department of Mechanical Engineering & Applied Mechanics, U. of Pennsylvania, 19104-6315 Philadelphia, PA, USA; vvasilo@seas.upenn.edu

<sup>2</sup>Department of Mechanical Engineering, National Technical University of Athens, 15780 Athens, Greece.; [kmach, egpapado]@central.ntua.gr.

$$I_r = m_r \cdot R^2 \quad (1)$$

The damping coefficients related with each leg prismatic and rotational joints and the reaction wheel rotational joint are  $b_l$ ,  $b_\varphi$  and  $b_r$  respectively. The body position in the sagittal plane and the pitch angle are denoted by  $(x, y)$  and  $\theta$  respectively. Each relative angle is denoted by  $\varphi$ , each absolute angle by  $\gamma$ , and each instantaneous length as  $l$ . The subscripts  $f$  and  $h$  correspond to the fore and the hind leg. The  $F_{g,f}$ ,  $F_{g,h}$  and  $F_{t,f}$ ,  $F_{t,h}$  represent the vertical and tangential forces (subscripts  $g$  and  $t$  respectively), exerted on each foot by the compliant ground.

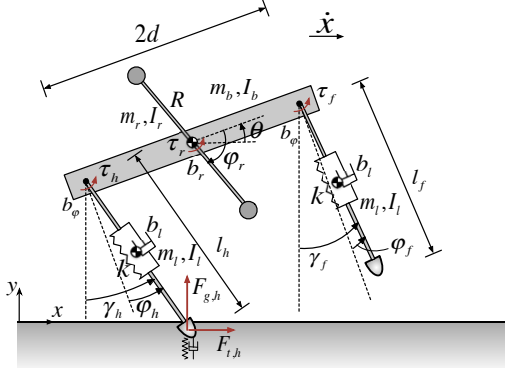


Figure 1. The dynamic model of the quadruped robot.

In deriving the equations of motion, the employed generalized coordinates include the body CoM position vector in the inertial frame  $(x, y)$ , the pitch angle of the body  $\theta$ , the relative angles  $\varphi_f$ ,  $\varphi_h$ , the length of the two legs  $l_f$ ,  $l_h$ , and finally the relative angle of the reaction wheel  $\varphi_r$ . Then, the equations of motion take the following form,

$$\mathbf{M}(\mathbf{q})\ddot{\mathbf{q}} + \mathbf{C}(\mathbf{q}, \dot{\mathbf{q}}) = \mathbf{B}\boldsymbol{\tau} + \mathbf{J}^T \mathbf{F} \quad (2)$$

where  $\mathbf{q}$  represents the configuration space as described above,  $\mathbf{M}(\mathbf{q})$  is a symmetric  $8 \times 8$  mass matrix,  $\mathbf{C}(\mathbf{q}, \dot{\mathbf{q}})$  is an  $8 \times 1$  vector containing gravity, centrifugal and Coriolis terms,  $\mathbf{B}$  assigns control inputs  $\boldsymbol{\tau}$  to  $\ddot{\mathbf{q}}$ , and the Jacobian  $\mathbf{J}$  maps the external forces from the ground  $\mathbf{F}$  to  $\mathbf{q}$ .

Many researchers consider legs of zero mass or inertia, keeping the body pitching unaffected during flight [3]. This is a rather severe assumption that does not reflect reality, and therefore it is not used for the simulation of the robot's motion here. Others control the pitch angle indirectly by driving the legs appropriately in stance or in aerial phase [7], [8]. However, this approach would require significant modifications in the analytically derived monopod controller, and the conclusions regarding stable locomotion on terrains with variable stiffness would be of no use here.

As a zero pitch angle is required for successful pronking, here this angle is controlled in the aerial phase using a reaction wheel. More specifically, since the legs are not considered massless, the conservation of angular momentum introduces a nonholonomic constraint that dictates a body rotation, when the motors position the legs to the desired touchdown angles. As a consequence, the legs do not hit the ground at the same time, and this disturbance turns pronking into a complex bounding gait, to which the monopod controller cannot safely adapt. Although a reaction wheel is a secondary control, and thus an optional system load, it can be widely used in many tasks besides pronking, increasing the

agility of general purpose legged machines. Therefore, we do not consider it as a special ad hoc device, but as a control input with wide applicability that can improve the performance of significantly underactuated legged robots.

### III. ACTUATOR MODEL

In the literature, most theoretical works and simulations do not include motor models, i.e the actuators are considered ideal torque sources. Several other works just introduce limits on torque and speed in the form of a speed-torque characteristic for the maximum supply voltage [11]. However, such models still conceal important information and do not reflect reality. For example, as will be shown next, the most important limits forming the operating range of an actuator system come from the gearbox mechanical limits and the current/voltage limits of the motor servoamplifier.

*Defining the limits of the actuator.* In this work, we focus on DC motors (brushed or brushless), since these are preferred in most robots that use electric actuation. In several applications, e.g. when backdrivability is required and thus a gearbox cannot be used, the operating range is bounded by the speed-torque characteristic corresponding to maximum supply voltage and by the current limit of the servoamplifier, see Fig. 2. However, in applications such as legged robotics, that demand significant torque in high speeds and thus need speed reduction, the actuator operating range is constrained mainly by the gearbox mechanical limits and the servoamplifier current/voltage limits. As a consequence, in many cases, a large region defined by the motor characteristic cannot be used and must be excluded in the analysis.

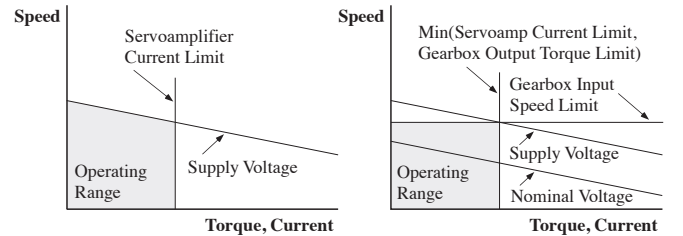


Figure 2. Left: The operating range of a DC motor without a gearbox. Right: Limited operating range of a DC motor with a gearbox.

More generally, the actual operating range of a drive train for such applications is hardly formed by the motor speed-torque characteristic. In fact, by regulating the supply voltage appropriately, this range does not depend on the motor's characteristic at all. It is noted that a DC motor can practically work at any voltage and the nominal voltage is just a reference, as long as the current remains within the thermal limits of the motor. For demanding loads, such as high torques in high speeds required in legged locomotion, an ideal supply voltage would be the one that defines a characteristic tangent to the limits of the gearbox to allow for maximum exploitation of the actuator, as shown in Fig. 2.

*Choice of the actuator reduction ratio.* For a gearmotor with rotor MoI  $I_{rotor}$ , gearbox reduction ratio  $n$  and MoI  $I_{gear}$  that drives a load with MoI  $I_{load}$ , the total MoI  $I_{eq}$  is,

$$I_{eq} = I_{load} + I_{gear} + n^2 I_{rotor} \quad (3)$$

The importance of (3) is apparent when choosing a reduction ratio to be used for legs that have significantly low MoI  $I_{load}$ . If a large reduction  $n$  is chosen, the total MoI would be primarily determined by the large term  $n^2 I_{rotor}$ . This will

result in greater disturbance on the main body attitude due to the conservation of angular momentum. Thus, the choice of the gearbox reduction ratio coupled with each hip actuator is a tradeoff problem between the required torques to push the body forward and the minimization of the total MoI  $I_{eq}$  so that body attitude disturbances during flight are minimized. On the other hand, the drive train of the reaction wheel must have a large total MoI  $I_{eq}$  to effectively adjust the body's pitch angle and reject any disturbances from leg positioning.

*Virtual Actuators.* Although modeling and analysis so far were performed using virtual legs, the previous discussion concerning the actuator model is valid only if a single actuator is used for each separate load. However, a virtual leg is in fact driven by two actuators working in parallel, e.g. the fore left motor and the fore right motor. Therefore, we introduce the concept of a *virtual actuator*, describing an actuator that is equivalent to two parallel ones and can be included safely in the analysis. The characteristics of these two identical motors have to be combined to yield the operating range of a virtual actuator. Combining the speed-torque lines of two motors in parallel will result in a characteristic with half the slope of that of the single motor as shown in the left of Fig. 3. Moreover, when a servoamplifier and a gearbox are also considered, the operating range of the virtual actuator occurs as a synthesis of the operating ranges of the two actuators, as depicted in the right of Fig. 3. These diagrams have the typical form given by most DC motor manufacturers, including a continuous operation region (low torque/current) and a short-term one (high torque/current).

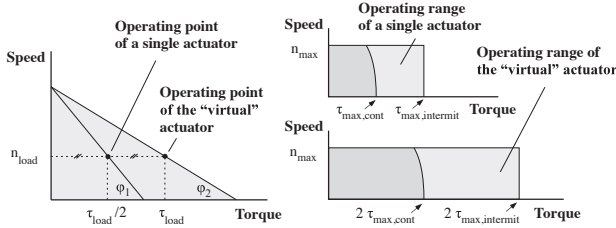


Figure 3. Speed-torque characteristic synthesis for two identical DC motors working in parallel into the equivalent of a virtual motor. Left: Speed-torque characteristic curves. Right: Operating ranges.

#### IV. FOOT-TERRAIN INTERACTION

To describe realistically the leg interaction with the deformable ground during its motion, the viscoplastic impact model proposed in [4] is employed. According to this model, the interaction force  $F_g$  at stance instance  $i$  is,

$$F_g^i(y_g, \dot{y}_g) = \begin{cases} F_c^i = (\lambda_c^i \cdot k_g + b_g \cdot \dot{y}_g)(y_g - y_e^{i-1})^n, & \dot{y}_g \geq 0 \\ F_r^i = (\lambda_r^i \cdot k_g + b_g \cdot \dot{y}_g)(y_g - y_e^i)^n, & \dot{y}_g < 0 \end{cases} \quad (4)$$

where subscripts  $c$ ,  $r$  stand for compression and restitution respectively,  $y_e$  is the reached impact depth,  $k_g$  and  $b_g$  are the stiffness and damping coefficients respectively,  $n$  in the case of Hertzian non-adhesive contact is 1.5, and  $y_g$  is the penetration depth. The equivalent stiffness  $k_g$  is related to the materials into contact, [12]. Damping is considered as a parameter affected by the stiffness [13], and given by

$$b_g = 1.5 \cdot c_a \cdot k_g \quad (5)$$

where throughout this work  $c_a = 0.2$ , without affecting the generality of the conclusions. The Coefficient of Permanent

Terrain Deformation  $\lambda$  accounts for the permanent deformation during successive impacts on the same horizontal point, and since the ground becomes stiffer during restitution,  $\lambda_r \geq \lambda_c \geq 1$ . The index  $i$  is used to identify an impact instance (stance), as the terrain inherits the characteristics from the previous impact instant. The coefficient recursive form and proposed model is presented in [4]. Finally, the depth  $y_e^i$  at the  $i^{th}$  impact can be calculated using the maximum compression,  $y_{c,max}^i$ , as follows,

$$y_e^i = y_{c,max}^i \cdot \left(1 - \sqrt{\lambda_c^i / \lambda_r^i}\right) + y_e^{i-1} \cdot \left(\sqrt{\lambda_c^i / \lambda_r^i}\right) \quad (6)$$

where  $y_e^0 = 0$  for consistency.

*Friction.* It is important to examine whether the foot of each leg, as it touches the ground, slips or sticks. For this reason, a friction description is required. Here, the Classical Coulomb friction model is used, which is an approximation of the standard Slip-stick friction model in terms of eliminating discontinuities at the static friction region that are unacceptable for simulation purposes [14]. This is achieved by adding a velocity threshold  $u_e$ , below which the foot is considered to stick. The friction force  $F_t$  is, thus, given by

$$F_t = \begin{cases} -\text{sgn} \dot{x}_g \cdot F_g \cdot \left[ \mu_c + (\mu_s - \mu_c) \cdot e^{-\frac{|\dot{x}_g|}{u_e}} \right], & |\dot{x}_g| > u_e \\ -\text{sgn} \dot{x}_g \cdot (\mu_s \cdot F_g) \cdot |\dot{x}_g \cdot u_e^{-1}|, & |\dot{x}_g| \leq u_e \end{cases} \quad (7)$$

where  $\dot{x}_g$  is the velocity component of the foot that is parallel to the tangential plane between the foot and the ground,  $F_g$  is the normal to the same plane interaction force from (4),  $\mu_c$  is the Coulomb (kinetic) friction coefficient,  $\mu_s$  is the Stribeck effect parameter. Without affecting the generality of the conclusions, we assume that  $u_e = 10^{-3}$  m/s and  $u_s = 10^{-2}$  m/s.

#### V. CONTROL METHODOLOGY

In [4], a novel controller for a monopod hopping robot on compliant terrains, called *Extended Multipart (x-MP)*, was presented. The controller is capable of achieving and retaining a desired forward speed and main body apex height on different terrains, with a *single* actuator located at the robot hip. In [4], it was shown also that this controller outperforms controllers designed for stiff terrains, as the terrain compliance increases. The approach taken in this paper is to use the main principle of this controller and extend its applicability to quadruped controller design.

The quadruped is required to run in a pronking gait, in which both the fore and hind virtual legs hit the ground at the same time. The controller acts just after both legs have left the ground, i.e. when the ground phase of stride  $j-1$  terminates and the flight phase of stride  $j$  begins. At that moment, it calculates a desired touchdown relative angle  $\varphi_{id}^j$  for both legs and two constant torques  $\tau_{s,f}^j$  and  $\tau_{s,h}^j$  to be applied by the fore and hind hip actuator respectively during the ground phase of stride  $j$  so that a specified forward speed  $\dot{x}_{des}$  and main body apex height  $h_{des}$  is reached. The controller acts in several steps as described in detail next.

*Estimation of equivalent controller parameters.* The first controller action is to map the behavior of the quadruped robot on compliant terrain, to a simple equivalent model of a

monopod robot, with a single actuator at its hip, on stiff terrain, as shown in Fig. 4, by calculating an equivalent mass, stiffness and damping coefficients  $M'$ ,  $k'$  and  $b'$  respectively. To achieve this, it is assumed that in pronking both legs touch and leave the ground at the same time without requiring any body pitching motion. The equivalent model is used for calculating the desired touchdown angle  $\varphi_{td}^j$  and constant stance torques  $\tau_{s,f}^j$  and  $\tau_{s,h}^j$ .

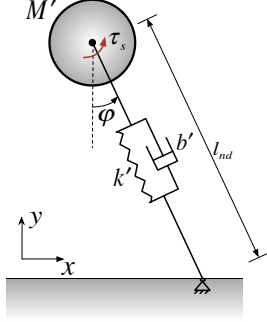


Figure 4. The equivalent monopod used in describing quadruped pronking.

Since the mass  $m_l$  of each leg is significantly smaller than the combined mass of the main body  $m_b$  and of the reaction wheel  $m_r$ , the equivalent mass  $M'$  that will be used in the control algorithm is given by,

$$M' = m_b + m_r \quad (8)$$

Following the methodology in [4], the calculation of  $k'$  and  $b'$  is based on previous stride response and energy losses due to damping and ground dissipation. Specifically, the duration  $\Delta t_s^{j-1}$  of the ground phase of stride  $j-1$  is taken equal to half of the natural period of a harmonic oscillation. Thus,  $k'$  is found as,

$$k' = \left( \pi / \Delta t_s^{j-1} \right)^2 \cdot M' \quad (9)$$

Taking into account that on a realistic terrain, there is no guarantee that the robot legs touch or leave the ground at exactly the same time, as small deviations may occur, the duration time  $\Delta t_s^{j-1}$  for the quadruped robot is considered to be equal to the time duration of the hind leg stance; the time duration of the front leg stance could have been chosen instead.

On the other hand, the equivalent damping  $b'$  is calculated as in [4], using force sensors located at each foot, and an estimate of the damping parameters to determine the energy  $E_{gdis}^{j-1}$  dissipated by the ground and the energy  $E_{damp}^{j-1}$  dissipated in the robot joints during the stride  $j-1$ .

*Calculation of touchdown angle and constant stance torque.* By calculating  $M'$ ,  $k'$  and  $b'$ , the quadruped robot behavior during pronking on *compliant* terrain is fully mapped to the behavior of a monopod hopping robot running on *stiff* terrain. Thus, a control method for this monopod robot would produce the same response in the quadruped robot. For this reason, the next action of the x-MP controller is to determine a desired touchdown angle  $\varphi_{td}^j$  and constant torque  $\tau_s^j$  to be applied during the next stance phase, so as to regulate the forward speed and apex height of the equivalent monopod in Fig 4. To do so, the controller exploits the hopping robot dynamics during stance, described by,

$$M' \cdot \ddot{x} + k' \cdot (L - l_{nd}) \cdot s\varphi - b' \cdot \dot{l}_{nd} \cdot s\varphi = -\tau_s^j \cdot l_{nd}^{-1} \cdot c\varphi \quad (10)$$

$$M' \cdot (\ddot{y} + g) - k' \cdot (L - l_{nd}) \cdot c\varphi + b' \cdot \dot{l}_{nd} \cdot c\varphi = -\tau_s^j \cdot l_{nd}^{-1} \cdot s\varphi \quad (11)$$

where  $c\varphi = \cos\varphi$ ,  $s\varphi = \sin\varphi$ ,  $l_{nd}$  is the instant length of the monopod at any time and  $\varphi$  is the monopod's relative angle which, since there is no pitching motion of the main body, coincides with its absolute angle. By integrating (10) and (11) with the method presented in [15], the touchdown angle  $\varphi_{td}^j$  and constant torque  $\tau_s^j$  are extracted, so that the monopod reaches a desired forward speed  $\dot{x}_{des}$  and body apex height  $h_{des}$ . It is noted, though, that the monopod has one actuator while the quadruped robot has two actuators. For this reason, the calculated torque  $\tau_s^j$  is equally distributed between each actuator so that the commanded torques at the fore and the hind hip actuator,  $\tau_{s,f}^j$  and  $\tau_{s,h}^j$ , are set as,

$$\tau_{s,f}^j = \tau_{s,h}^j = 0.5 \cdot \tau_s^j \quad (12)$$

Following these calculations, the legs are servoed to the touchdown relative angle  $\varphi_{td}^j$  during the flight phase using a PD controller as described in [4]. After the touchdown of each leg, which is determined using a force sensor at each robot foot, the constant torques  $\tau_{s,f}^j$  and  $\tau_{s,h}^j$  are applied.

*Control of the reaction wheel.* To achieve the desired pronking gait, both legs must touch the ground at the same time instant. Since the touchdown angle is the same for both the fore and the hind leg, this can be ensured by regulating the body pitch angle to zero during the flight phase in order to reject any deviations in the body attitude occurring due to the conservation of angular momentum while positioning the legs. To this end, a PD controller is employed as follows

$$\tau_r^f = k_{p,r} \cdot (\theta_{des} - \theta) + k_{d,r} \cdot (\dot{\theta}_{des} - \dot{\theta}) \quad (13)$$

where  $\theta_{des} = 0$  and  $\dot{\theta}_{des} = 0$  are the desired pitch angle and pitch velocity respectively. The gains are chosen so that the response is fast without overshooting.

However, the torque  $\tau_r^f$  applied during the flight phase results in acceleration of the reaction wheel, which may lead to rotational speed saturation or failure of its gearbox. For this reason, the reaction wheel must be decelerated during the ground phase, when both legs are in contact with the ground and there is no need for pitch control. Thus at double stance, a virtual brake is applied according to the following equation

$$\tau_r^s = -k_{d,r} \cdot \dot{\varphi}_r \quad (14)$$

*Sensing.* The controller uses data from force sensors yielding the ground reaction forces, from two encoders at each leg that measure the relative angle  $\varphi$  and leg length  $l$ , and estimates of the body position and attitude  $(x, y, \theta)$  using the robot model fused with data from an inertial sensor, [4]. No additional sensor for the terrain properties is required.

## VI. RESULTS

To evaluate the controller during pronking and under alternative scenarios, a number of simulations were carried out. The equivalent stiffness  $k_g$  between the materials in contact (i.e. foot and ground) was used [12], where the properties of various terrains were found in [16]. An ether polyurethane foot was selected with Young's modulus  $E = 100 \text{ MPa}$ . As an example, the equivalent stiffness between this material and granite with  $E = 50 \text{ GPa}$  is  $k_g \approx 450,000 \text{ N/m}$ . Hence, three main categories of terrains were examined: *soft* ground with  $k_g = 8 \cdot 10^4 \text{ N/m}$ ,  $\mu_s = 0.5$ ,  $\mu_c = 0.4$ , *moderate* ground with  $k_g = 2 \cdot 10^5 \text{ N/m}$ ,  $\mu_s = 0.6$ ,  $\mu_c = 0.5$ , and *stiff* ground with  $k_g = 4 \cdot 10^5 \text{ N/m}$ ,  $\mu_s = 0.7$ ,  $\mu_c = 0.6$ . The acceleration of gravity was  $g = 9.81 \text{ m/s}^2$ .

In all cases, the quadruped parameters were:  $m_b = 10 \text{ kg}$ ,  $I_b = 1.0 \text{ kgm}^2$ ,  $d = 0.27 \text{ m}$ ,  $m_l = 0.6 \text{ kg}$ ,  $I_l = 0.0045 \text{ kgm}^2$ ,  $m_r = 1.0 \text{ kg}$ ,  $R = 0.25 \text{ m}$ ,  $L = 0.30 \text{ m}$ ,  $k = 12,000 \text{ N/m}$ . The damping coefficients were  $b_l = 2 \text{ Ns/m}$ ,  $b_\varphi = 0.2 \text{ Nms}$  and  $b_r = 0.1 \text{ Nms}$ . The same DC motor was used for both legs and the reaction wheel but with different reduction ratios, according to the design principles discussed in Section III. In more detail, the motor MoI was  $I_{rotor} = 33.3 \text{ gcm}^2$ , with a speed-torque gradient  $869 \text{ rpm/mNm}$  and stall torque  $1020 \text{ mNm}$ . To supply large torques, the wheel motor gearbox had a reduction ratio of 51:1,  $I_{gear} = 0.7 \text{ gcm}^2$  and maximum output torque  $\tau_{max} = 7.5 \text{ Nm}$ , while the gearbox used for each leg actuation had a reduction ratio of 14:1,  $I_{gear} = 0.7 \text{ gcm}^2$  and maximum permissible torque  $\tau_{max} = 3.75 \text{ Nm}$ . The permissible input speed for both gearboxes was 8000 rpm, and the maximum permissible motor servoamplifier current was 12 A. For the reaction wheel controller, the values of  $k_{p,r} = 700$  and  $k_{d,r} = 40$  were selected as they allow the controller to be fast enough to change the pitch angle before the next touchdown, while avoiding excessive oscillations and overshooting.

The simulations were performed in Matlab using ode23s with absolute tolerance  $10^{-5}$ , relative tolerance  $10^{-4}$  and maximum step  $10^{-4}$ . To minimize the zero-crossing arithmetic problems created by the numerical stiffness, the impact was considered over when the interaction force between the foot and the terrain was below 5N.

*Controller performance with varying desired forward velocity.* Fig. 5 displays the controller response on compliant terrain with varying desired forward velocity and constant desired apex height. As can be seen, the controller closely follows the commanded objectives, with some deviation of around 0.08 m/s in the forward velocity and almost no error in the desired main body apex height. Apart from that, the controller successfully achieved to generate a pronking gait, as shown in the Hildebrand diagram, depicted in Fig. 6. It can be concluded that both the fore and the hind leg hit the ground together and take off with negligible time difference (of about 0.85% of stride duration), mainly caused by the reaction wheel deceleration during the ground phase.

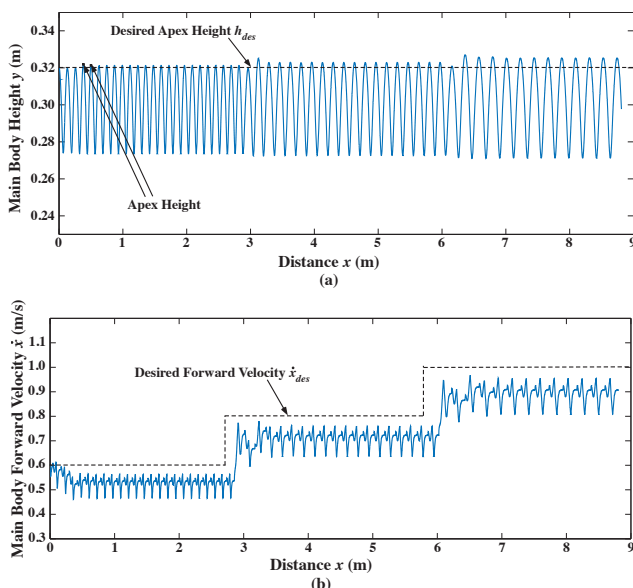


Figure 5. Controller performance on rough terrain with varying desired forward velocity: (a) Main Body Height, (b) Forward Velocity.

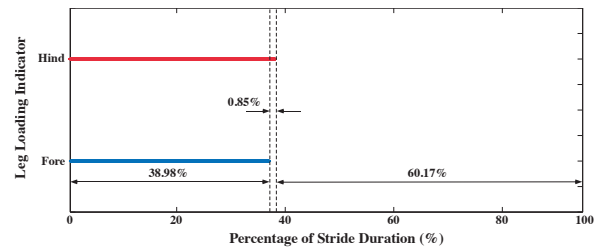


Figure 6. Hildebrand diagram of the quadruped robot during one stride.

*Controller performance with varying desired main body apex height.* In Fig. 7 the controller response on compliant terrain with varying desired apex height and constant desired forward velocity is shown. Again, the controller manages to achieve the desired objectives with satisfactory accuracy.

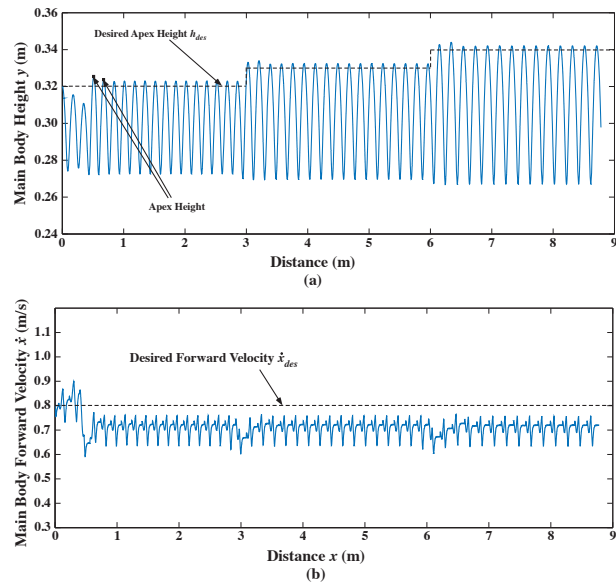


Figure 7. Controller performance on rough terrain with varying desired apex height: (a) Main Body Height, (b) Forward Velocity.

*Controller performance with varying terrain properties.* Finally, the controller was tested on several terrain types with different compliance and permanent deformations and was commanded to retain a constant desired forward velocity of 0.6 m/s and main body apex height of 0.32 m, as shown in Fig. 8. During each part of the designated path, the contact stiffness and shape deformation (shown by the max  $\lambda = [1+a(i)]$  in the figure) were changed abruptly. The controller adapts quickly to each terrain and follows the commanded objectives, as illustrated in Fig. 8. Small deviations occur on severely compliant terrains with large permanent deformations, where the motors reach more easily their saturation levels. These results provide an excellent example of how gearbox and servoamplifier limits really affect robot motion. The mapping from the quadruped to an equivalent monopod is not perfect; such deviations are more visible on more compliant terrains.

Apart from the controller performance under different scenarios, it is necessary to examine whether the motion of the reaction wheel was stable from stride to stride. This is a crucial factor for the total system stability, as a constant reaction wheel acceleration could result in motor saturation and, eventually, in total gait failure. For the same reasons, the main body pitch angle must perform an oscillation around

zero, so that a pronging gait is preserved. Both of these requirements were met by the controller, as shown in Fig. 9.

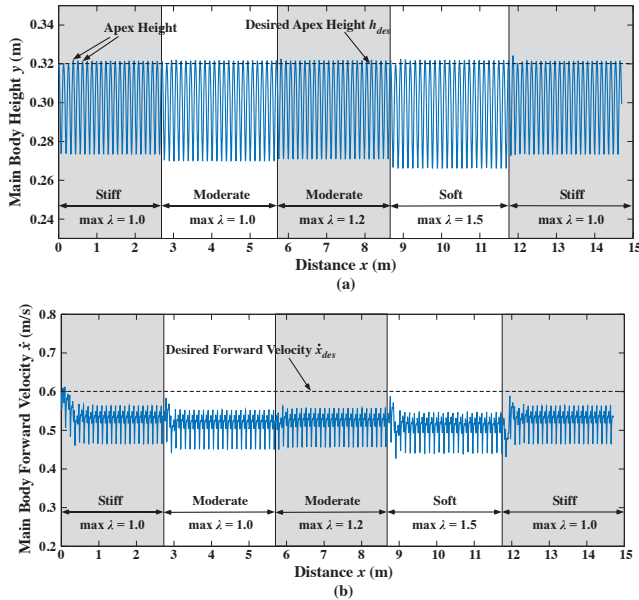


Figure 8. Controller performance on different terrains with specified desired velocity and apex height: (a) Main Body Height, (b) Forward Velocity.

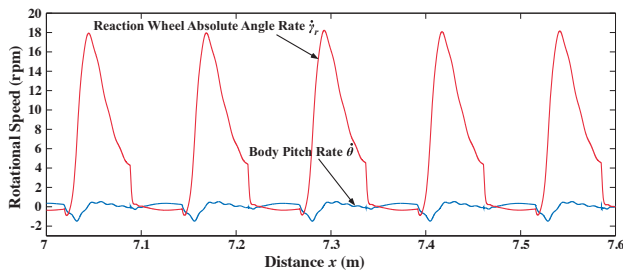


Figure 9. Evolution of the reaction wheel angle rate and the body pitch angle rate while traversing moderate terrain with small deformations.

Finally, it is useful to depict graphically whether and when actuators reach saturation and, more importantly, whether all their operating points lie within the specified limits. As an example, Fig. 10 depicts the results for the reaction wheel and the front leg actuator during the run presented in Fig. 8. As can be seen, no gearbox torque-speed bounds are violated; the reaction wheel was torque saturated occasionally while decelerating.

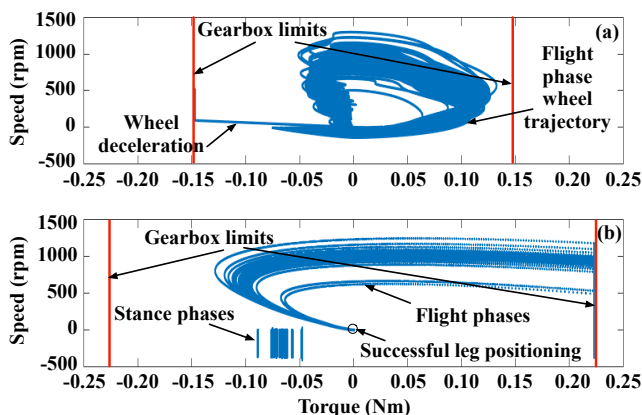


Figure 10. Operating points and limits of: (a) the reaction wheel actuator and (b) the front leg actuator.

The front leg actuator reached saturation at the beginning of each flight interval, when trying to position the leg forward; however, leg positioning was successful.

## VII. CONCLUSION

In this work, the motion of a quadruped robot during pronging was examined using our controller for even compliant terrains. To retain a desired pitch during pronging, a reaction wheel was employed. The dynamics of the motor drivetrains for both the leg hip joints and the reaction wheel were incorporated, and the concept of virtual actuators was introduced that must be considered in models that use virtual legs. The controller developed for the monopod case, was modified appropriately for the quadruped robot. Simulation results showed good performance in reaching the apex height and forward velocity goals on various terrains, thus demonstrating that the developed controller is effective.

## REFERENCES

- [1] Kalakrishnan, K. et al, "Fast Robust Quadruped Locomotion over Challenging Terrain", *IEEE Int. Conf. on Robotics and Automation (ICRA '10)*, May 2010, Anchorage, Alaska, USA, pp. 2665-2670.
- [2] Gehring, C. et al, "Control of Dynamic Gaits for a Quadrupedal Robot", *IEEE Int. Conf. on Robotics and Automation (ICRA '13)*, May 2013, Karlsruhe, Germany, pp. 3287-3292.
- [3] Park, H., et al., "Quadruped Bounding Control with Variable Duty Cycle via Vertical Impulse Scaling," *IEEE/RSJ Int. Conf. Int. Robots & Systems (IROS '14)*, Chicago, IL, USA, 2014, pp. 3245-3252.
- [4] Vasilopoulos, V., Paraskevas, I. S. and Papadopoulos, E. G., "Compliant Terrain Legged Locomotion Using a Viscoplastic Approach", *IEEE/RSJ Int. Conf. on Intelligent Robots and Systems (IROS '14)*, Chicago, Illinois, USA, September 2014, pp. 4849-4854.
- [5] Wu, A., and Geyer, H., "Highly Robust Running of Articulated Bipedes in Unobserved Terrain," *IEEE/RSJ Int. Conf. on Intelligent Robots and Systems*, Chicago, Illinois, USA, 2014, pp. 2558-2565.
- [6] Li, C., Zhang, T., and Goldman, D.I., "A terradynamics of legged locomotion on granular media," *Science*, 339(6126), pp.1408-1412, 2013.
- [7] Raibert, M., *Legged Robots That Balance*, MIT Press, Cambridge, MA, 1986.
- [8] Cherouvim, N. and Papadopoulos, E., "Pitch Control for Running Quadrupeds Using in Flight Leg Positioning," *Proc. 15<sup>th</sup> IEEE Mediterranean Conference on Control and Automation*, June 27-29, 2007, Athens, Greece.
- [9] Briggs, Randall, et al. "Tails in biomimetic design: Analysis, simulation, and experiment." *Proc. IEEE Int. Conf. on Intell. Robots and Systems (IROS '12)*, 2012, Algarve, Portugal, pp. 1473-1480.
- [10] De, A. and Koditschek, D. E., "Parallel composition of templates for tail-energized planar hopping", *IEEE Int. Conf. on Robotics and Automation (ICRA '15)*, Seattle, WA, May 2015, pp. 4562-4569.
- [11] Talebi, S., Poulakakis, I., Papadopoulos, E., and Buehler, M., "Quadruped Robot Running With a Bounding Gait," in *Experimental Robotics VII*, Rus, D., and Singh, S., (Eds.), Lecture Notes in Control and Information Sciences Series, Springer-Verlag, 2001.
- [12] Johnson, K. L., *Contact mechanics*, Cambridge Univ. Press, 1977.
- [13] Marhefka, D. W. and Orin, D. E., "A compliant contact model with nonlinear damping for simulation of robotic systems," *IEEE Transactions on Systems, Man, and Cybernetics-part A: Systems and Humans*, vol. 29, no. 6, pp. 566-572, 1999.
- [14] Haessig, D. A. and Friedland, B., "On the Modeling and Simulation of Friction", *American Control Conference*, San Diego, CA, USA, 1990.
- [15] Cherouvim, N. and Papadopoulos, E., "Control of Hopping Speed and Height Over Unknown Rough Terrain Using a Single Actuator," *IEEE Int. Conf. on Robotics and Automation (ICRA '09)*, Kobe, Japan, May 2009, pp. 2743-2748.
- [16] Zhu, T., "Some Useful Numbers on the Engineering Properties of Materials", [online], <http://goo.gl/pY8jeK> (Acc.: 4 February 2015).